Journal of Molecular Structure 1181 (2019) 428–435

Contents lists available at ScienceDirect

Journal of Molecular Structure

journal homepage: http://www.elsevier.com/locate/molstruc

In silico study of febuxostat analogs as inhibitors of xanthine oxidoreductase: A combined 3D-QSAR and molecular docking study

Xiaolei Li [1], Haiyan Zhou [1], Xianwei Mo, Lei Zhang, Jing Li*

School of Bioscience and Bioengineering, South China University of Technology, Guangzhou, 510006, PR China

ARTICLE INFO

Article history:
Received 25 June 2018
Received in revised form
3 January 2019
Accepted 4 January 2019
Available online 7 January 2019

Keywords:
Xanthine oxidoreductase inhibitors
Molecular docking
3D-QSAR
Topomer CoMFA

ABSTRACT

We explored molecular docking and a three-dimensional quantitative structure-activity relationship (3D-QSAR) model of 107 xanthine oxidoreductase (XOR) inhibitors containing a phenyl-substituted five-membered heterocycle. Molecular-docking results showed that Arg880, Phe914, and Phe1009 might be potential active residues targeted by the 107 XOR inhibitors evaluated in this study. Topomer comparative molecular field analysis (CoMFA) ($q^2 = 0.571$; $r^2 = 0.833$) was used for 3D-QSAR. The results indicated that benzene substituted with moderately bulky substituents, a cyano group, and a five-membered heterocycle with a carboxyl group might enhance XOR inhibitory activity. Four new compounds were designed based on these results, and each exhibited potential XOR inhibitory activity *in vitro*.

1. Introduction

Xanthine oxidoreductase (XOR) is a target for treatment of gout and conditions associated with hyperuricemia [1–3]. In 1966, allopurinol (Fig. 1), a structural isomer of hypoxanthine, was the first XOR inhibitor marketed for treatment of gout and other hyperuricemia-associated conditions. However, allopurinol and its analogs have severe life-threatening side-effects, collectively called "allopurinol intolerance syndrome" [4,5]. Febuxostat is a thiazole-carboxylic acid derivative that inhibits XOR activity, approved by the US Food and Drug Administration (FDA) for treatment of gout in 2009 [6]. Owing to its excellent potency and better toxicological profile, many febuxostat analogs have been designed, with a primary focus on replacement of the thiazole group with other five-membered heterocycles, such as triazole [7], imidazole [8], selenazoles [9], pyrazoles (e.g., Y-700) [10], and isoxazoles [11] (Fig. 1).

To better understand the mechanisms of XOR inhibition by febuxostat and febuxostat analogs, and to guide the design of novel XOR inhibitors, it is necessary to evaluate febuxostat analogs with reported half-maximal inhibitory concentration (IC_{50}) values to determine generic structure-activity relationships (SARs) for XOR inhibitors with a phenyl-substituted five-membered heterocycle [7–11]. In the current study, a generic 3D-QSAR model of a series of compounds was established by Topomer CoMFA [12–14]. In parallel, a molecular docking study was performed to gain insight into binding interactions between XOR and febuxostat-related XOR inhibitors.

2. Materials and methods

2.1. Computer simulations

The research procedures used in this study are shown in Fig. 2. Data preparation, ligand-based study (3D-QSAR model), and receptor-based study (molecular docking) were the three main components of this study.

2.1.1. Data set

A series of febuxostat analogs that act as XOR inhibitors, and their biologic activities, were obtained through a literature search and used as a dataset for molecular modeling [7–11,15–18]. Among these 107 inhibitors, the range of IC_{50} values was 0.0014–26.13 μM, suggesting that the diversity in the dataset was sufficient to construct stable 3D-QSAR models. The pIC_{50} [$pIC_{50} = -\log (IC_{50}/10^6)$] values for these inhibitors ranged from 4.58 to 8.85. Based on

Abbreviations: XOR, xanthine oxidoreductase; 3D-QSAR, three-dimensional quantitative structure-activity relationship; CoMFA, comparative molecular field analysis; IC_{50}, half-maximal inhibitory concentration; SARs, structure-activity relationships; PDB, Protein Data Bank.

* Corresponding author.
E-mail address: lij@scut.edu.cn (J. Li).

[1] These authors contributed equally to this work and should be considered as co-first authors.

https://doi.org/10.1016/j.molstruc.2019.01.017
0022-2860/

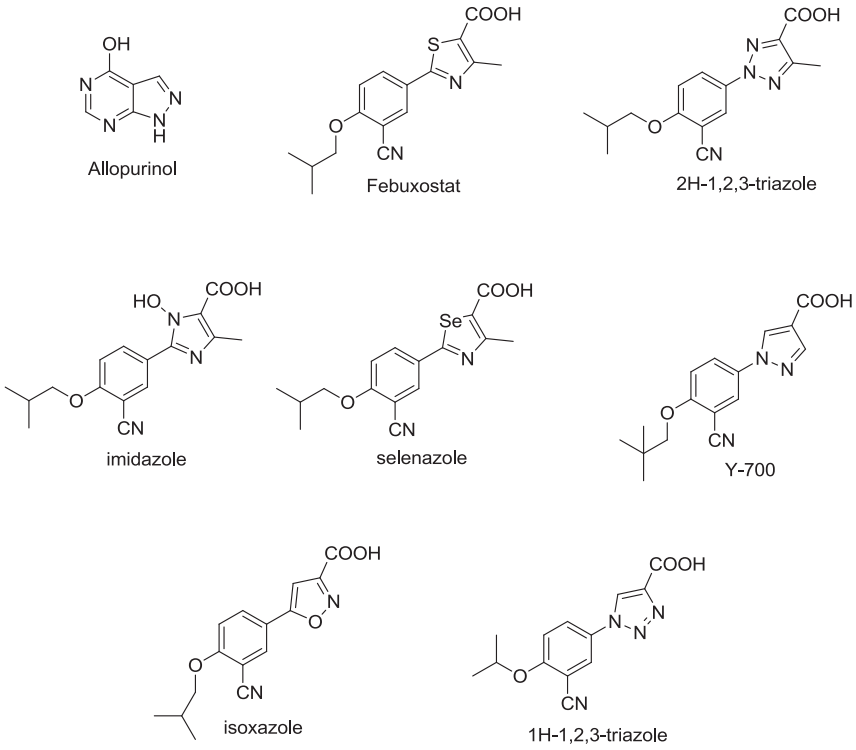

Fig. 1. Chemical structures of selected XOR inhibitors.

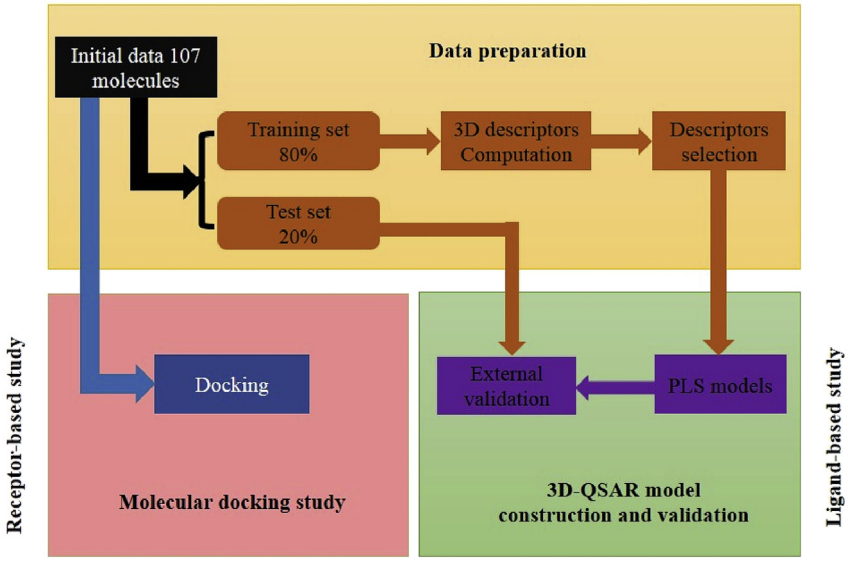

Fig. 2. Flowchart for computational drug design.

pIC_{50} values, the inhibitors were divided into two sets at an approximate ratio of 4:1, with 86 compounds assigned to the training set and 21 compounds assigned to the test set, (Table S1) [19].

2.1.2. Topomer CoMFA modeling

All 2D structures were sketched in ChemDraw Ultra v8.0.3 (PerkinElmer, Waltham, MA, USA). They were converted into 3D structures using SYBYL-X 2.0 (Tripos Software, Saint Louis, MO, USA) running on Windows™ 7.0 64-bit operating system. All parameters of Topomer CoMFA methods were default values except for those specifically mentioned. Using Tripos force field, energy minimizations were performed using the Powell method when the numerical value met the energy convergence criterion of 0.005 kcal/mol A. The independent variables were Topomer CoMFA descriptors and the dependent variables were pIC_{50} values [20].

2.1.3. Model validation

To assess the predictability and reliability of the 3D-QSAR models, both internal validation and external validation were performed. For internal validation, the partial least squares [21–24] algorithm was used to determine the optimal number of

components by leave-one-out cross-validation [25], and defined the highest cross-validation correlation coefficient (q^2) to be:

$$q^2 = 1 - \sum \left(Y_{pred} - Y_{exp}\right)^2 \Big/ \sum \left(Y_{exp} - Y_{mean}\right)^2$$

where Y_{pred}, Y_{exp}, and Y_{mean} represented the predicted, experimental, and mean biologic activities of training-set compounds, respectively. For external validation, the predicted correlation coefficient r^2_{pred} [26–28] reflected the ability to predict 3D-QSAR models and defined r^2_{pred} as:

$$r^2_{pred} = (SD - PRESS)/SD$$

where SD expressed the sum of the squared deviation between the molecular biological activity of the test set and the molecular mean biological activity of the training set, and PRESS was the sum of squares between the predictions and the experimental biological activity of the test set molecules [29].

2.1.4. Molecular docking

To further study binding interactions between the crucial groups of febuxostat analogs and XOR, molecular docking was performed using SYBYL-X 2.0 (Surflex-Dock method) [30]. The protein structures of XOR complexed with Y-700 were taken from the Research Collaboration for Structural Bioinformatics Protein Data Bank (PDB ID: 1VDV) (www.rscb.org/pdb) and used in docking experiments [31]. Before docking, the "Prepare Protein Structure" procedure was used to prepare the inputted XOR structures for docking, which comprised extracting the ligand Y-700, removing all the watery molecules, and adding polar hydrogen atoms to the XOR receptor [32]. Meanwhile, the "Ligand Structure Preparation" procedure was used to prepare the inputted ligands for docking, which comprised removing duplicates, adding polar hydrogen atoms, and generating 3D conformations. Docking simulations were carried out using a standard Surflex-Dock protocol with default values for adjustable parameters [33].

2.2. XOR inhibitors design and activity evaluation

To further verify the reliability of molecular docking and 3D-QSAR models, new XOR inhibitors were designed, synthesized, XOR inhibitory activities evaluated *in vitro*.

2.2.1. Chemistry

Based on our previous studies [15], synthesis of compounds **a-d** is shown in Scheme 1. Commercially available 5-bromo-2-fluorobenzonitrile (**1**) was treated with Na_2S to provide **2**. Compound **2** was alkylated with C3–C6 alkyl halides in the presence of K_2CO_3 to give **3a-d**. Through a C–N coupling reaction and hydrolysis, target compounds **a-d** were obtained from **3a-d**.

2.2.2. Experimental protocols

2.2.2.1. General information. ^{1}H NMR and ^{13}C NMR spectra were recorded in $CDCl_3$ or DMSO-d6 on Bruker Avance III HD 400 MHz spectrometers (Bruker, Germany) using TMS as the internal standard, respectively. Chemical shifts (δ) were reported in ppm with respect to TMS. Infrared spectra were recorded on a Bruker Vertex 33 instrument (Bruker, Germany). HRMS spectra were recorded on an Agilent 1290 instrument in ESI mode (Agilent Technologies, USA). All the reaction progress were checked on by thin layer chromatography (TLC) using silica gel glass cards (Qingdao Ocean Chemical, Qingdao, Shandong, P. R. China) with UV light indicator at 254 nm. Silica gel column chromatography was performed using 200–300 mesh of silica gel with the indicated solvents as the eluent. Unless otherwise indicated, commercially available reagents were used without further purification.

*2.2.2.2. General procedures for the synthesis of compounds **a-d***

*2.2.2.2.1. The preparation of 5-bromo-2-mercaptobenzonitrile (**2**).* A mixture of compound **1** (3.0 g, 15 mmol), Na_2S (1.3 g, 16.5 mmol), and DMF (10 mL) was stirred at room temperature for 5.0 h. The resulting mixture was treated with NaOH (1 M, 300 mL) and stirred for 0.5 h. Then the mixture was added EtOAc (200 mL). The organic layer was separated, and the aqueous phase was extracted with EtOAc (100 mL × 2). After that, the water phase was acidified with 6 M HCl solution to pH = 2 and extracted with EtOAc (100 mL × 2). The combined organic layer was washed with brine (300 mL × 2), dried over anhydrous $MgSO_4$, filtered and evaporated. The residue was purified by flash column chromatography (0–10% EtOAc/petroleum ether) to afford **2** as yellow solid (31.2%); ^{1}H NMR ($CDCl_3$) δ 7.78 (d, J = 2.0 Hz, 1H, Ar–H), 7.71 (dd, J = 2.0, 8.6 Hz, 1H, Ar–H), 7.63 (d, J = 8.6 Hz, 1H, Ar–H).

*2.2.2.2.2. General procedure for the preparation of compounds **3a-d**.* A mixture of K_2CO_3 (1.0 g, 7.0 mmol), 5-bromo-2-mercaptobenzonitrile (**2**) (0.5 g, 2.3 mmol) in DMF (10 mL) was added in a 100 mL reaction vial, which was sealed and stirred at room temperature for 1.0 h. Then the reaction mixture was allowed to add alkyl halide (7.0 mmol) and heated at 60 °C for 6 h. The mixture was cooled to room temperature and diluted with H_2O (30 mL), the resulting mixture was added EtOAc (30 mL). The organic layer was separated, and the aqueous phase was extracted with EtOAc (20 mL × 3). The combined organic layers were washed with brine (100 mL × 2), dried over anhydrous Na_2SO_4 and evaporated in a vacuum. Afterward, the residue was purified by flash column chromatography (5% EtOAc/petroleum ether) to afford the desired product **3a-d**.

5-bromo-2-(isopropylthio)-benzonitrile (**3a**). Colourless oil (yield: 35.6%); ^{1}H NMR ($CDCl_3$) δ 7.76 (d, 1H, J = 2.2 Hz, Ar–H), 7.62 (dd, 1H, J = 2.2, 8.5 Hz, Ar–H), 7.37 (d, 1H, J = 8.5 Hz, Ar–H),

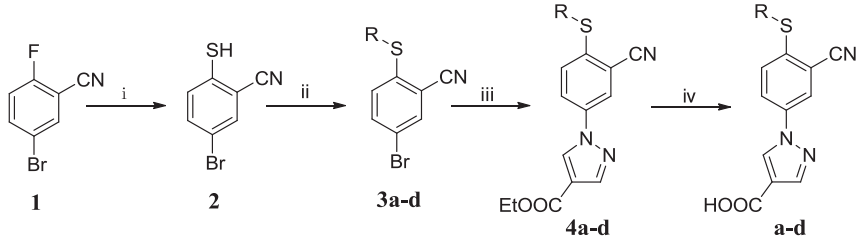

a. R=$CH(CH_3)_2$ **b**. R=$CH_2CH(CH_3)_2$

c. R=$CHCH_3CH_2CH_3$ **d**. R=$CH_2CH(CH_2CH_3)_2$

Scheme 1. Reagents and conditions: (i) Na_2S, DMF, NaOH, CH_2Cl_2; (ii) K_2CO_3, DMF, alkyl halide, 50 °C; (iii) K_2CO_3, CuI, ethyl 1H-pyrazole-4-carboxylate, (*E*)–N, N′-dimethyl-1, 2-cyclohexane-diamine, DMF, 110 °C; (iv) NaOH aq. (1 M), THF/ethanol (1:1), 60 °C, HCl aq. (1 M), rt.

3.60–3.46 (m, 1H, CH(CH$_3$)$_2$), 1.34 (d, 6H, J = 6.7 Hz, CH(CH$_3$)$_2$).

5-bromo-2-(isobutylthio)-benzonitrile (**3b**). Colourless oil (yield: 54.7%); ^{1}H NMR (CDCl$_3$) δ 7.65 (d, 1H, J = 2.2 Hz, Ar–H), 7.54 (dd, 1H, J = 2.2, 8.6 Hz, Ar–H), 7.20 (d, 1H, J = 8.6 Hz, Ar–H), 2.82 (m, 2H, J = 5.3 Hz, CH$_2$CH(CH$_3$)$_2$), 1.93–1.75 (m, 1H, CH$_2$CH(CH$_3$)$_2$), 1.10–0.92 (d, 6H, J = 6.7 Hz, CH$_2$CH(CH$_3$)$_2$).

5-bromo-2-(sec-butylthio)-benzonitrile (**3c**). Colourless oil (yield: 53.9%); ^{1}H NMR (CDCl$_3$) δ 7.74 (d, 1H, J = 2.2 Hz, Ar–H), 7.61 (dd, 1H, J = 2.2, 8.5 Hz, Ar–H), 7.35 (d, 1H, J = 8.5 Hz, Ar–H), 3.40–3.27 (m, 1H, CHCH$_3$CH$_2$CH$_3$), 1.74–1.52 (m, 2H, CHCH$_3$CH$_2$CH$_3$), 1.31 (d, 3H, J = 6.7 Hz, CHCH$_3$CH$_2$CH$_3$), 1.06–0.98 (t, 3H, J = 6.4 Hz, CHCH$_3$CH$_2$CH$_3$).

5-bromo-2-((2-ethylbutyl)thio)-benzonitrile (**3d**). Colourless oil (yield: 48.3%); ^{1}H NMR (CDCl$_3$) δ 7.71 (s, 1H, Ar–H), 7.60 (d, J = 8.5 Hz, 1H, Ar–H), 7.26 (d, J = 6.7 Hz, 1H, Ar–H), 2.97 (d, J = 5.7 Hz, 1H, CH$_2$CH(CH$_2$CH$_3$)$_2$), 1.60 (s, 2H, CH$_2$CH(CH$_2$CH$_3$)$_2$), 1.57–1.43 (m, 4H, CH$_2$CH(CH$_2$CH$_3$)$_2$), 0.90 (t, J = 7.2 Hz, 6H, CH$_2$CH(CH$_2$CH$_3$)$_2$).

*2.2.2.2.3. General procedure for the preparation of compounds **4a-d**.* Under the nitrogen atmosphere, a mixture of compounds **3a-d** (0.24 g, 1.0 mmol), 1H-pyrazole-3-carboxylate (0.11 g, 0.8 mmol), K_2CO_3 (0.23 g, 1.7 mmol), (*E*)–N, N′-Dimethyl-1, 2-cyclohexanediamine (82 mg, 0.96 mmol), CuI (15 mg, 0.08 mmol) in DMF (5 mL) were added in 25 mL reaction vial, which was heated to 110 °C and stirred for 24 h. Then the reaction mixture was cooled to room temperature and diluted with H_2O (20 mL), the resulting mixture was added EtOAc (20 mL). The organic layer was separated, and the aqueous phase was extracted with EtOAc (15 mL × 3). The combined organic extracts were washed with brine (50 mL), dried over anhydrous Na_2SO_4. After that, the organic phase was concentrated in a vacuum and was purified by flash column chromatography (6–12% EtOAc/petroleum ether) to afford the desired products **4a-d**.

Ethyl 1-(3-cyano-4-(isopropylthio)phenyl)-1H-pyrazole-4-carboxylate (**4a**). White solid (yield: 98.0%); ^{1}H NMR (CDCl$_3$) δ 8.44 (s, 1H, CH), 8.13 (s, 1H, CH), 8.05 (d, 1H, J = 2.5 Hz, Ar–H), 7.89 (dd, 1H, J = 2.5, 8.6 Hz, Ar–H), 7.64 (d, 1H, J = 8.7 Hz, Ar–H), 4.37 (q, 2H, J = 7.1 Hz, CH$_2$CH$_3$), 3.62 (m, 1H, CH(CH$_3$)$_2$), 1.44–1.40 (overlap, 3H, CH$_2$CH$_3$), 1.41–1.35 (d, 6H, J = 1.4 Hz, CH(CH$_3$)$_2$).

Ethyl 1-(3-cyano-4-(isobutylthio)phenyl)-1H-pyrazole-4-carboxylate (**4b**). White solid (yield: 58.7%); ^{1}H NMR (CDCl$_3$) δ 8.39 (s, 1H, CH), 8.10 (s, 1H, CH), 7.98 (d, 1H, J = 2.4 Hz, Ar–H), 7.84 (dd, 1H, J = 2.5, 8.7 Hz, Ar–H), 7.49 (d, 1H, J = 8.7 Hz, Ar–H), 4.34 (q, 2H, J = 7.1 Hz, CH$_2$CH$_3$), 2.93 (d, 2H, J = 6.8 Hz, CH$_2$CH(CH$_3$)$_2$), 1.92 (m, 1H, CH$_2$CH(CH$_3$)$_2$), 1.38 (t, 3H, J = 7.1 Hz, CH$_2$CH$_3$), 1.08 (d, 6H, J = 6.7 Hz, CH$_2$CH(CH$_3$)$_2$).

Ethyl 1-(4-(sec-butylthio)-3-cyano-phenyl)-1H-pyrazole-4-carboxylate (**4c**). White solid (yield: 60.7%); ^{1}H NMR (CDCl$_3$) δ 8.41 (s, 1H, CH), 8.11 (s, 1H, CH), 8.02 (d, J = 2.4 Hz, 1H, Ar–H), 7.86 (dd, J = 8.7, 2.5 Hz, 1H, Ar–H), 7.60 (d, 1H, J = 8.7 Hz, Ar–H), 4.34 (q, 2H, J = 7.1 Hz, CH$_2$CH$_3$), 3.39 (m, 1H, CHCH$_3$CH$_2$CH$_3$), 1.79–1.56 (m, 2H, CHCH$_3$CH$_2$CH$_3$), 1.38 (t, 3H, J = 7.1 Hz, CH$_2$CH$_3$), 1.34 (d, 3H, J = 4.7 Hz, CHCH$_3$CH$_2$CH$_3$), 1.05 (t, 3H, J = 7.4 Hz, CHCH$_3$CH$_2$CH$_3$).

Ethyl 1-(3-cyano-4-((2-ethylbutyl) thio) phenyl)-1H-pyrazole-4-carboxylate (**4d**). White solid (yield: 58.2%); ^{1}H NMR (CDCl$_3$) δ 8.36 (s, 1H, CH), 8.07 (s, 1H, CH), 7.95 (d, J = 2.4 Hz, 1H, Ar–H), 7.81 (dd, J = 8.7, 2.5 Hz, 1H, Ar–H), 7.47 (d, J = 8.7 Hz, 1H, Ar–H), 4.31 (q, J = 7.1 Hz, 2H, CH$_2$CH$_3$), 2.99 (d, J = 6.0 Hz, 2H, CH$_2$CH(CH$_2$CH$_3$)$_2$), 1.54 (dd, J = 10.9, 4.8 Hz, 1H, CH$_2$CH(CH$_2$CH$_3$)$_2$), 1.46 (tdd, J = 8.9, 7.1, 3.0 Hz, 4H, CH$_2$CH(CH$_2$CH$_3$)$_2$), 1.34 (t, J = 7.1 Hz, 3H, CH$_2$CH$_3$), 0.88 (t, J = 7.4 Hz, 6H, CH$_2$CH(CH$_2$CH$_3$)$_2$).

*2.2.2.2.4. General procedure for the preparation of compounds **a-d**.* **4a-d** (0.12 g, 0.38 mmol) in the mixed solvent of THF (5 mL) ethanol (5 mL) was added in a 50 mL reaction vial, which was sealed and heated at 60 °C until TLC revealed that conversion of **4a-d** was completed. Then the reaction mixture was allowed to cool to room temperature and acidified with 1 M HCl to pH = 1–2 in ice water. The reaction mixture was diluted with H_2O, the suspension was stirred in ice water for 20 min, obtained the crude product by filtration. The crude product was purified by washing with water and recrystallizing in methanol to afford the desired product **a-d**.

1-(3-cyano-4-(isopropylthio) phenyl)-1H-pyrazole-4-carboxylic acid (**a**). White solid (yield:100%); ^{1}H NMR (DMSO-d6) δ 8.87 (s, 1H, CH), 8.16 (s, 1H, CH), 7.96 (d, 1H, J = 8.7 Hz, Ar–H), 7.88 (s, 1H, Ar–H), 7.54 (d, 1H, J = 8.7 Hz, Ar–H), 3.47 (m, 1H, CH(CH$_3$)$_2$), 1.07 (d, J = 6.5 Hz, 6H, CH(CH$_3$)$_2$); ^{13}C NMR (DMSO-d6) δ 163.8, 143.0, 138.7, 137.8, 132.8, 132.1, 124.3, 124.1, 118.2, 116.9, 114.8, 38.4, 23.0; HRMS: Calcd for $C_{14}H_{13}N_3O_2S$ $[M+Na]^+$ 310.0629, Found 310.0633.

1-(3-cyano-4-(isobutylthio) phenyl)-1H-pyrazole-4-carboxylic acid (**b**). White solid (yield: 82.9%); ^{1}H NMR (DMSO-d6) δ 12.74 (s, 1H, COOH), 9.13 (s, 1H, CH), 8.40 (d, 1H, J = 2.5 Hz, CH), 8.22–8.18 (dd, 1H, J = 2.0, 8.2 Hz, Ar–H), 8.12 (s, 1H, Ar–H), 7.73 (d, 1H, J = 8.9 Hz, Ar–H), 3.05 (d, 2H, J = 6.8 Hz, CH$_2$CH(CH$_3$)$_2$), 1.92–1.76 (m, 1H, CH$_2$CH(CH$_3$)$_2$), 1.02 (d, 6H, J = 6.6 Hz, CH$_2$CH(CH$_3$)$_2$); ^{13}C NMR (DMSO-d6) δ 163.8, 142.9, 140.7, 137.1, 132.0, 130.0, 124.4, 118.1, 116.8, 112.6, 41.4, 28.1, 22.0; HRMS: Calcd for $C_{15}H_{15}N_3O_2S$ $[M+Na]^+$ 324.0777, Found 324.0779.

1-(4-(sec-butylthio)-3-cyanophenyl)-1H-pyrazole-4-carboxylic acid (**c**). White solid (yield: 88.5%); ^{1}H NMR (DMSO-d6) δ 11.85 (s, 1H, COOH), 8.28 (s, 1H, CH), 7.55 (s, 1H, CH), 7.34 (dd, J = 2.5, 8.8 Hz, 1H, Ar–H), 7.26 (s, 1H, Ar–H), 6.92 (d, J = 8.8 Hz, 1H, Ar–H), 2.69 (q, J = 6.5 Hz, 1H, CHCH$_3$CH$_2$CH$_3$), 0.75 (m, 2H, CHCH$_3$CH$_2$CH$_3$), 0.42 (d, J = 6.7 Hz, 3H, CHCH$_3$CH$_2$CH$_3$), 0.12 (t, J = 7.4 Hz, 3H, CHCH$_3$CH$_2$CH$_3$); ^{13}C NMR (DMSO-d6): δ 163.8, 143.0, 138.7, 137.8, 132.9, 132.1, 124.1, 118.2, 116.9, 114.9, 44.9, 29.3, 20.5, 11.5; HRMS: Calcd for $C_{15}H_{15}N_3O_2S$ $[M+Na]^+$ 324.0777, Found 324.0786.

1-(3-cyano-4-((2-ethylbutyl) thio) phenyl)-1H-pyrazole-4-carboxylic acid (**d**). White solid (yield: 87.7%); ^{1}H NMR (DMSO-d6) δ 12.75 (s, 1H, COOH), 9.14 (s, 1H,CH), 8.41 (s, 1H, CH), 8.20 (d, J = 8.8 Hz, 1H, Ar–H), 8.13 (s, 1H, Ar–H), 7.74 (d, J = 8.8 Hz, 1H, Ar–H), 3.12 (d, J = 5.9 Hz, 2H, CH$_2$CH(CH$_2$CH$_3$)$_2$), 1.52 (dt, J = 6.1, 11.9 Hz, 1H, CH$_2$CH(CH$_2$CH$_3$)$_2$), 1.48–1.38 (m, 4H, CH$_2$CH(CH$_2$CH$_3$)$_2$), 0.87 (t, J = 7.2 Hz, 6H, CH$_2$CH(CH$_2$CH$_3$)$_2$; ^{13}C NMR (DMSO-d6) δ 163.81, 142.92, 140.70, 137.11, 132.01, 130.06, 124.31, 123.96, 118.14, 116.76, 112.67; HRMS: Calcd for $C_{17}H_{19}N_3O_2S$ $[M+H]^+$ 330.1276, Found 330.1257.

2.2.3. Biological activity in vitro

Xanthine (0.5 mM) and 0.5 mL/100 mL XOR (Sigma, from bovine milk) were prepared by diluting in PBS (PBS refers to 1× PBS unless otherwise specified). The required concentrations of compounds **a-d** were prepared in PBS and used for XOR activity assays. According to the procedure reported by Fukunari et al. [31], XOR activity with xanthine as substrate was measured spectrophotometrically as follows. A blank solution (PBS), enzyme solution (100 μL), and test compounds were added to a 96 well plate, then incubated for 3 min at 37 °C. Following incubation, substrate solution was immediately added to the plate. Samples were monitored at 295 nm every 30 s for 5 min using an Ensipre-2300 microplate reader (Perkin Elmer, USA). IC_{50} values were calculated using Excel 2007 and Prism 6.0 statistical software (GraphPad Software, Inc., San Diego, CA).

3. Results and discussion

3.1. 3D-QSAR and docking analyses

3.1.1. Data processing

As shown in Fig. 3, 107 compounds with “high,” “moderate,” and “low” activity were selected in approximately equal proportions in

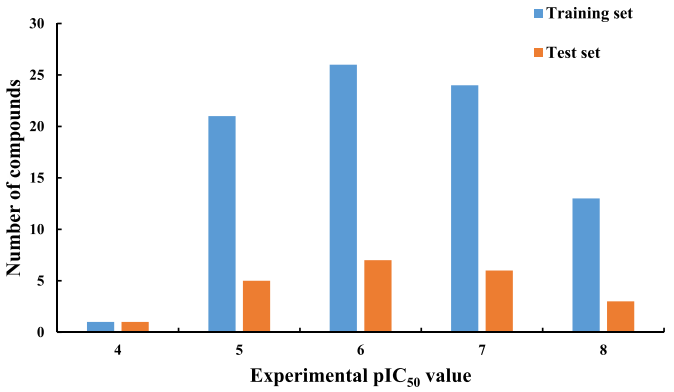

Fig. 3. Distribution of inhibitory activities for the training set and test set in Topomer CoFMA studies.

both the training set and test set by considering the distribution of biologic data and structural diversity to ensure that the datasets used for 3D-QSAR modeling were appropriate.

3.1.2. Topomer CoMFA

In general, the splitting mode of the R-group is important for model generation in Topomer CoMFA. As such, comparison of two different splitting modes was performed (Fig. 4). Inhibitor structure (Table S1) showed the substituent group at R_2 to be −CN, suggesting that the molecules could be split into three pieces: R_1, R_3, and R_2-substituted benzene. However, by comparing the values of q^2 and r^2 (Table 1), it was clear that splitting the compounds into four pieces was more appropriate to our analyses.

3.1.3. Validation of 3D-QSAR models

The predicted pIC_{50} [$pIC_{50} = -\log (IC_{50}/10^6)$] values, including the training and test sets, their residual values, and contributions of R_1, R_2, and R_3 fragments, were calculated (Table S2). After obtaining an r^2_{pred} value of 0.656 from the test set, the predictive ability of the 3D-QSAR model was evaluated, and the robustness of the model was evaluated by external verification. The scatterplot in Fig. 5 showed that the predicted pIC_{50} values of those compounds were coincident with experimental values. These results demonstrated that the Topomer CoMFA model was reliable for predicting pIC_{50} values.

In addition, by comparing the fragment contribution values of R_1, R_2, and R_3, we hypothesized that substitution at R_2 had the greatest impact on XOR inhibitory activity, followed by R_1 and R_3.

3.1.4. 3D contour maps

To facilitate analyses, febuxostat was chosen as the reference in

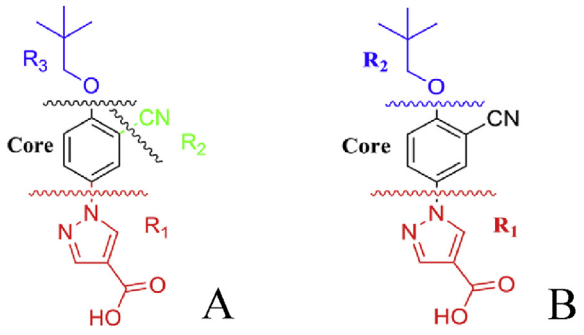

Fig. 4. The method of splitting compounds into pieces: (A) four pieces and (B) three pieces.

Table 1
Statistical analyses of the two methods of splitting molecules.

Method	q^2	r^2	N
Three pieces	0.537	0.789	5
Four pieces	0.571	0.833	5

q^2 = leave-one-out cross-validation correlation coefficient.
r^2 = Non-cross-validation correlation coefficient.
N = optional number of components.

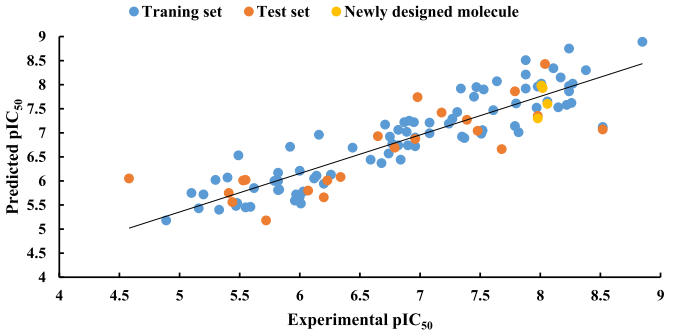

Fig. 5. Scatterplot of experimental *versus* predicted pIC_{50} values of training and test sets in a 3D-QSAR model.

3D coefficient contour maps (Fig. 6 and Fig. 7). Results of Topomer CoMFA models were interpreted graphically using field contribution maps. Fig. 7 shows the calculated Topomer CoMFA steric and electrostatic contour maps. Steric field analysis suggested that only moderately bulky substituents would be favorable, as shown by the green contours of the R_1 group, while bulky substituents would not contribute to inhibition, as shown by the yellow contours. These characteristics may explain higher activity of compound **20** ($pIC_{50} = 8.52$) with a butoxyl group as R_1, and lower activity of compounds **17** ($pIC_{50} = 6.26$) and **26** ($pIC_{50} = 5.92$) with -methoxyl and -octyloxyl R_1 groups, respectively (R_2 and R_3 were identical for these compounds). In electrostatic field, the advantage of negatively charged groups was indicated by red contours of R_1 group, with the advantage of positively charged groups indicated by blue contours. This phenomenon occurred because all R_1 substituents contained hetero atoms such as oxygen, nitrogen, and sulfur.

As shown in Fig. 7c, red contours at the R_2 group suggested that negatively charged groups would be favorable. Among the 107 compounds, compound **51** was the only one in which R_2 was a

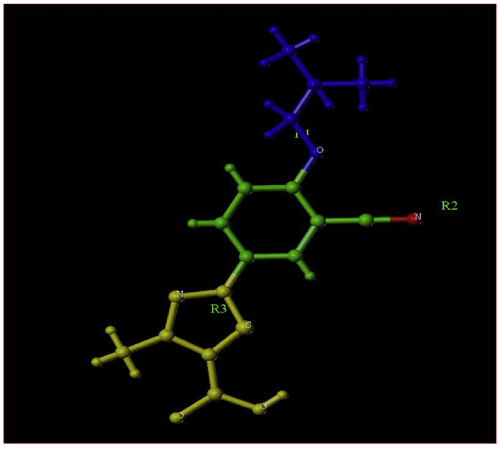

Fig. 6. Splitting of febuxostat.

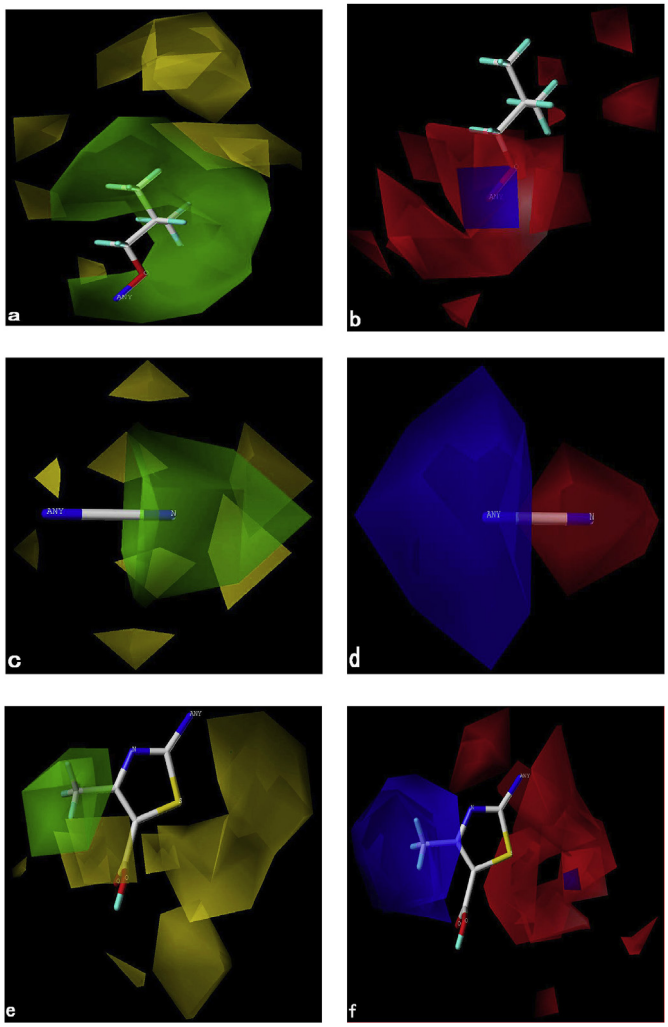

Fig. 7. CoMFA StDev * Coeff contour maps for febuxostat. (a) and (b) Steric and electrostatic field maps of the R_1 fragment, respectively. (c) and (d) Steric and electrostatic field maps of the R_2 fragment, respectively. (e) and (f) Steric and electrostatic field maps of the R_3 fragment, respectively (green and yellow contours denote sterically favorable and unfavorable sites, respectively; blue and red contours denote regions that favor electropositive and electronegative groups, respectively).

hydrogen, and this compound exhibited poor XOR inhibitory activity ($pIC_{50} = 5.33$). Nearly all other compounds had a cyano group or a nitro group at R_2.

Yellow contours at the R_3 group (between the benzene ring and S atom on the R_3 group) suggested that bulky substituents would be unfavorable at this site. This could explain significant reduction in XOR inhibitory activity for compound **21** ($pIC_{50} = 8.52$) and compound **28** ($pIC_{50} = 5.92$). Similarly, only moderately bulky substituents between the N atom and carboxyl group allowed for inhibitory activity. Finally, red contours at the R_3 group demonstrated that all R_3 substituents contained a carboxyl group as an essential group.

3.1.5. Docking analyses

To validate docking accuracy, co-crystalized ligand (Y-700) was first re-docked to the active binding site of XOR (PDB ID: 1VDV, www.rscb.org/pdb). As shown in Fig. 8, the occupied space and conformation of the re-docked moieties were closely associated with those of the co-crystalized moieties, suggesting acceptable reliability of the docking procedure. As shown in Fig. 9, binding

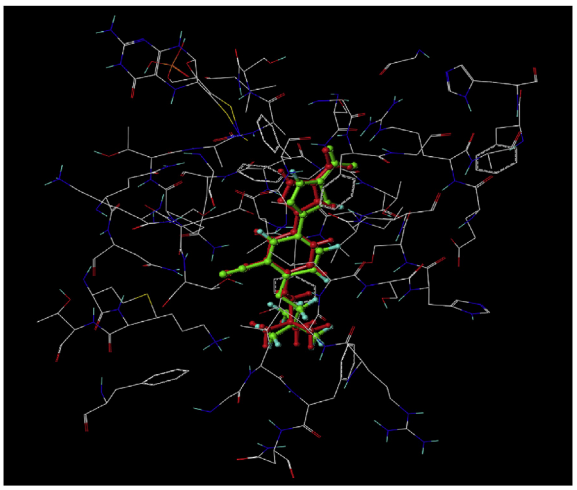

Fig. 8. Structural super-positioning of the co-crystal structure (green) and re-docked structure (red) for XOR.

between Y-700 and XOR had four main features (docking score: −6.309): 1) the carboxyl group extended to the catalytic center containing a molybdenum atom, and interacted with Arg880 (O—H—N: 2.33 Å, O—H—N: 1.97 Å) and Thr1010 (O—H—N: 2.22 Å) via hydrogen bonding; 2) the pyrazole ring was sandwiched between Phe914 (3.77 Å, 13.3°) and Phe1009 (4.69 Å, 69.4°) by π-π stacking; 3) the hydrogen bond between the −CN group and Asn768 (N—H—N: 2.44 Å); 4) R_1 occupied the channel through which the substrate enters the catalytic center of XOR, a hydrophobic pocket composed of phe 649, leu 648, lys 771, Val 1011, leu 1014, and phe 1013. Compound **61** (docking score: −7.343), another ligand with high XOR inhibitory activity, exhibited a similar interaction with XOR to that of Y-700, including hydrogen bonds with Arg880 (O—H—N: 2.19 Å, O—H—N: 1.74 Å), Thr1010 (O—H—N: 2.38 Å), and Asn768 (N—H—N: 2.64 Å) and π-π stacking between Phe914 (6.04 Å, 8.8°) and Phe1009 (4.83 Å, 70.0°).

3.2. XOR inhibitors design and activity evaluation

Based on the results from molecular docking and 3D-QSAR models, four new XOR inhibitors **a**-**d** were designed by choosing pyrazoles as the five-membered heterocycles. The experimental IC_{50} values, experimental pIC_{50} values, and predicted pIC_{50} values determined by Topomer CoMFA modeling are shown in Table 2. These results showed that predicted pIC_{50} values were consistent with experimental values. In addition, with increasing R_1 volume, changes in XOR inhibitory activity were in agreement with our hypothesis that only moderately bulky substituents at R_1 were favorable for XOR inhibition. Experimental IC_{50} values, experimental pIC_{50} values, and predicted pIC_{50} values determined by Tomoper CoMFA modeling are summarized in Table 2.

4. Conclusion

A combined computational and experimental approach was employed in this study to identify the structural determinants and specific binding modes between XOR and its inhibitors. Higher statistical values ($q^2 = 0.571$; $r^2 = 0.833$) suggested strong reliability and predictive capability of the Topomer CoMFA model. Receptor-based molecular docking studies suggested that hydrogen bonding, π-π stacking, and hydrophobic interactions were the most important interactions between XOR and its inhibitors. Furthermore, four newly designed compounds showed potential XOR

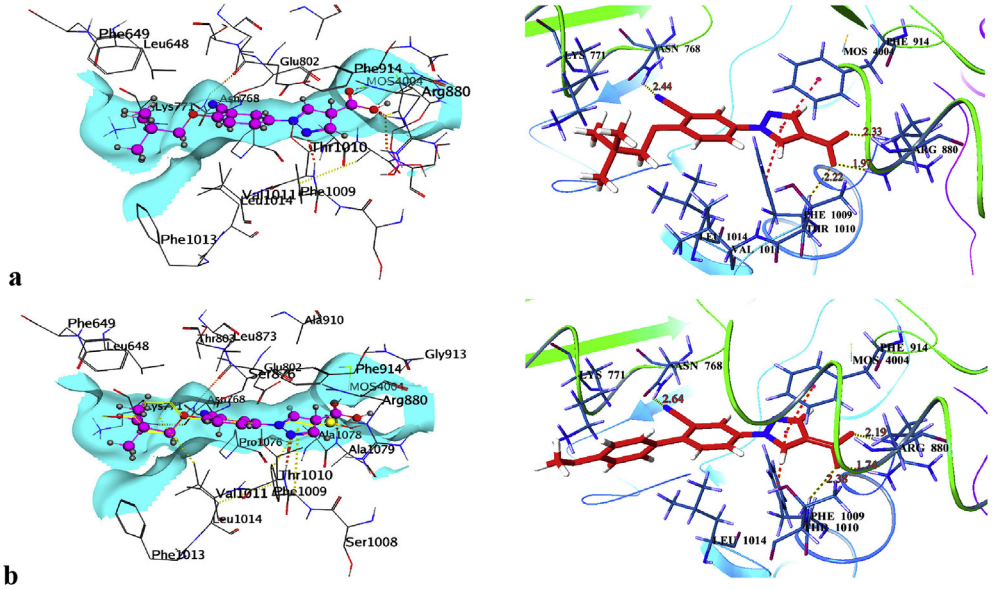

Fig. 9. Interactions between compounds and XOR protein residues. (a) Y-700 forms H-bonds with Arg880, Thr1010, and Asn768. (b) Compound **61** forms H-bonds with Arg880, Thr1010, and Asn768. (The docking graphics were created by MOE and polished by photoshop CS6).

Table 2
Values for IC_{50} and Predicted pIC_{50} on XOR for compounds **a**-**d**.

Compd.	R_1	IC_{50} (nM)[a]	Exp. pIC_{50}	Pred. pIC_{50}
a	$-SCH(CH_3)_2$	10.4	7.98	7.30
b	$-SCH_2CH(CH_3)_2$	9.8	8.01	7.98
c	$-SCHCH_3CH_2CH_3$	8.8	8.06	7.60
d	$-SCH_2CH(CH_2CH_3)_2$	9.6	8.02	7.93

[a] Values are the mean of three experiments.

inhibitory activity *in vitro*, with predicted pIC_{50} values that were consistent with experimental values. In conclusion, the QSAR and docking models obtained in this study could provide better virtual screening for design of febuxostat analogs, and indicated future research directions, such as further exploration of hydrophobic interactions and π-π stacking.

Conflicts of interest

The authors declare no conflict of interest.

Acknowledgments

This work was supported by the Science and Technology Project of Guangdong Province (2015A020211005) and the Guangzhou Science Technology and Innovation Commission (201704020036).

Appendix A. Supplementary data

Supplementary data to this article can be found online at https://doi.org/10.1016/j.molstruc.2019.01.017.

References

[1] D.T. Lowenthal, The treatment of hyperuricemia, Am. Fam. Physician 14 (1976) 98–100.
[2] E. Roddy, M. Doherty, Treatment of hyperuricaemia and gout, Clin. Med. 13 (2013) 400–403.
[3] F. Borges, E. Fernandes, F. Roleira, Progress towards the discovery of xanthine oxidase inhibitors, Curr. Med. Chem. 9 (2002) 195–217.
[4] K. Okamoto, B.T. Eger, T. Nishino, S. Kondo, E.F. Pai, T. Nishino, An extremely potent inhibitor of xanthine oxidoreductase crystal structure of the enzyme-inhibitor complex and mechanism of inhibition, J. Biol. Chem. 278 (2003) 1848–1855.
[5] G. Biagi, I. Giorgi, F. Pacchini, O. Livi, V. Scartoni, Cheminform abstract: 2-alkyloxyalkylthiohypoxanthines as new potent inhibitors of xanthine oxidase, IL Farmaco 56 (2001) 809–813.
[6] J.U. Song, S.P. Choi, T.H. Kim, C.K. Jung, J.Y. Lee, S.H. Jung, G.T. Kim, Design and synthesis of novel 2-(indol-5-yl)thiazole derivatives as xanthine oxidase inhibitors, Bioorg. Med. Chem. Lett 25 (2015) 1254–1258.
[7] A. Shi, D. Wang, H. Wang, Y. Wu, H. Tian, Q. Guan, K. Bao, W. Zhang, Synthesis and bioevaluation of 2-phenyl-5-methyl-2H-1, 2, 3-triazole-4-carboxylic acid/carbohydrazide derivatives as potent xanthine oxidase inhibitors, RSC Adv. 6 (2016) 114879–114888.
[8] S. Chen, T. Zhang, J. Wang, F. Wang, H. Niu, C. Wu, S. Wang, Synthesis and evaluation of 1-hydroxy/methoxy-4-methyl-2-phenyl-1H-imidazole-5-carboxylic acid derivatives as non-purine xanthine oxidase inhibitors, Eur. J. Med. Chem. 103 (2015) 343–353.
[9] G. Qi, Z. Cheng, X. Ma, L. Wang, D. Feng, Y. Cui, B. Kai, W. Lan, W. Zhang, Synthesis and bioevaluation of 2-phenyl-4-methyl-1, 3-selenazole-5-carboxylic acids as potent xanthine oxidase inhibitors, Eur. J. Med. Chem. 85 (2014) 508–516.
[10] S. Ishibuchi, H. Morimoto, T. Oe, T. Ikebe, H. Inoue, A. Fukunari, M. Kamezawa, I. Yamada, Y. Naka, Synthesis and structure-activity relationships of 1-phenylpyrazoles as xanthine oxidase inhibitors, Bioorg. Med. Chem. Lett 11 (2001) 879–882.
[11] S. Wang, J. Yan, J. Wang, J. Chen, T. Zhang, Y. Zhao, M. Xue, Synthesis of some 5-phenylisoxazole-3-carboxylic acid derivatives as potent xanthine oxidase inhibitors, ChemInform 45 (2010) 2663–2670.
[12] A.K. Halder, S.A. Amin, T. Jha, S. Gayen, Insight into the structural requirements of pyrimidine-based phosphodiesterase 10A (PDE10A) inhibitors by multiple validated 3D QSAR approaches, SAR QSAR Environ. Res. 28 (2017) 253–273.
[13] R.D. Cramer, Topomer CoMFA: a design methodology for rapid lead optimization, J. Med. Chem. 46 (2003) 374–388.
[14] C. Xu, Y. Ren, Molecular modeling studies of [6, 6, 5] tricyclic fused oxazolidinones as FXa inhibitors using 3D-QSAR, Topomer CoMFA, molecular docking and molecular dynamics simulations, Bioorg. Med. Chem. Lett 25 (2015) 4522–4528.
[15] J. Li, F. Wu, X. Liu, Y. Zou, H. Chen, Z. Li, L. Zhang, Synthesis and bioevaluation of 1-phenyl-pyrazole-4-carboxylic acid derivatives as potent xanthine oxidoreductase inhibitors, Eur. J. Med. Chem. 140 (2017) 20–30.
[16] T.J. Zhang, Q.X. Wu, S.Y. Li, L. Wang, Q. Sun, Y. Zhang, F.H. Meng, H. Gao, Synthesis and evaluation of 1-phenyl-1H-1, 2, 3-triazole-4-carboxylic acid derivatives as xanthine oxidase inhibitors, Bioorg. Med. Chem. Lett 27 (2017) 3812–3816.
[17] A. Šmelcerović, K. Tomović, Š. Žaklina, Ž. Petronijević, G. Kocić, T. Tomašič, Ž. Jakopin, M. Anderluh, Xanthine oxidase inhibitors beyond allopurinol and febuxostat; an overview and selection of potential leads based on in silico calculated physico-chemical properties, predicted pharmacokinetics and toxicity, Eur. J. Med. Chem. 135 (2017) 491–516.
[18] S.L.D. Silva, S. Marangoni, K.C. Weber, P. Homem-De-Mello, K.M. Honório,

A.B.F.D. Silva, A multivariate study on the inhibition of the xanthine oxidase by phenylpyrazole compounds, Int. Electron. J. Mol. Des. 4 (2005) 515–526.
[19] J.T. Leonard, K. Roy, On selection of training and test sets for the development of predictive QSAR models, Qsar Comb. Sci. 25 (2010) 235–251.
[20] Y. Xiang, Z. Hou, Z. Zhang, Pharmacophore and QSAR studies to design novel histone deacetylase 2 inhibitors, Chem. Biol. Drug Des. 79 (2012) 760–770.
[21] P. Geladi, Notes on the history and nature of partial least squares (PLS) modelling, J. Chemom. 2 (2010) 231–246.
[22] P. Geladi, B.R. Kowalski, Partial least-squares regression: a tutorial, Anal. Chim. Acta 185 (1985) 1–17.
[23] B.L. Bush, R.B. Nachbar, Sample-distance partial least squares: PLS optimized for many variables, with application to CoMFA, J. Com Aid Mol. Des. 7 (1993) 587–619.
[24] M. Clark, R.D.C. Iii, N.V. Opdenbosch, Validation of the general purpose tripos 5.2 force field, J. Comput. Chem. 10 (1989) 982–1012.
[25] C.R. 3Rd, D.E. Patterson, J.D. Bunce, Recent advances in comparative molecular field analysis (CoMFA), Prog. Clin. Biol. Res. 291 (1989) 161–165.
[26] A. Golbraikh, A. Tropsha, Beware of q2!, J. Mol. Graph. Model. 20 (2002) 269–276.
[27] R.D. Cramer, D.E. Patterson, J.D. Bunce, Comparative molecular field analysis (CoMFA). 1. Effect of shape on binding of steroids to carrier proteins, J. Am. Chem. Soc. 110 (1988) 5959–5967.
[28] E. Vrontaki, G. Melagraki, T. Mavromoustakos, A. Afantitis, Searching for anthranilic acid-based thumb pocket 2 HCV NS5B polymerase inhibitors through a combination of molecular docking, 3D-QSAR and virtual screening, J. Enzym. Inhib. Med. Chem. 31 (2016) 38–52.
[29] C.Z. Hao, S.W. Xia, H. Wang, J. Xue, L. Yu, Using 3D-QSAR and molecular docking insight into inhibitors binding with complex-associated kinases CDK8, J. Mol. Struct. 1173 (2018) 498–511.
[30] P.S. Ambure, R.P. Gangwal, A.T. Sangamwar, 3D-QSAR and molecular docking analysis of biphenyl amide derivatives as p38 mitogen-activated protein kinase inhibitors, Mol. Divers. 16 (2012) 377–388.
[31] A. Fukunari, K. Okamoto, T. Nishino, B.T. Eger, E.F. Pai, M. Kamezawa, I. Yamada, N. Kato, Y-,700 [1-[3-Cyano-4-(2, 2-dimethylpropoxy)phenyl]-1H-pyrazole-4-carboxylic acid]: a potent xanthine oxidoreductase inhibitor with hepatic excretion, J. Pharmacol. Exp. Therapeut. 311 (2004) 519–528.
[32] G.W. Van, J.P. Overington, A ligand's-eye view of protein similarity, Nat. Methods. 10 (2013) 116–117.
[33] A. Ghaleb, A. Aouidate, M. Ghamali, A. Sbai, M. Bouachrine, T. Lakhlifi, 3D-QSAR modeling and molecular docking studies on a series of 2, 5 disubstituted 1, 3, 4-oxadiazoles, J. Mol. Struct. 1145 (2017) 278–284.